Cancer diagnosis by microscopic axial super-resolving reconstruction approach of cytological and histological images

Zeev Zalevsky
Bar-Ilan University
School of Engineering
Ramat-Gan 52900, Israel

Eran Rosmann
Tel-Aviv University
Faculty of Engineering
69978 Tel-Aviv, Israel

Edmond Sabo
Carmel Medical Center
Department of Pathology
34362 Haifa, Israel

Ehud Rivlin
Technion—Israel Institute of Technology
Computer Science Deptartment
3200 Haifa, Israel

David Mendlovic
Tel-Aviv University
Faculty of Engineering
69978 Tel-Aviv, Israel

Abstract. We present an optical data reconstruction method to be used for cancer diagnostics via cytological and histological images. The approach allows realizing extended depth of focus and data compression using wavelet transformation that is realized optically with very low computational complexity. The extended depth of focus and the compressed images are generated out of a set of optically defocused images realized due to axial translation of the diagnosed sample. The extended depth of focus image may be used for 3-D cytological information display without stereo projection. Note that the extended depth of focus actually means super-resolving imaging, since getting out of focus means filtering the high band spatial frequencies within the image. © *2006 Society of Photo-Optical Instrumentation Engineers.* [DOI: 10.1117/1.2336413]

Subject terms: medical imaging; data compression; focus.

Paper 050841 received Oct. 22, 2006; accepted for publication Jan. 23, 2006; published online Sep. 1, 2006.

1 Introduction

3-D information, depth of focus, and compression are very significant in improving pathological capabilities. 3-D microscopy has been investigated before, however, the techniques were mainly based on stereoscopic vision[1,2] or holographic recordings and confocal microscopy.[3–5] All those approaches either provide nonsufficient resolution in the depth axis, vary the operation procedures of the pathologists, or require very expensive additions on top of the existing diagnostic station. In regular microscopy, increase in the spatial resolution decreases the focal depth. In Ref. 6, Carrington proposed an interesting image restoration method that is suitable for images with missing or truncated data. This method is applied on 3-D optically sectioned microscope images of fluorescently labeled cells. This approach uses the out-of-focus information, allowing the author to subdivide a large image into smaller pieces without a substantial edge effect.

Cancer diagnosis is usually performed by the examination of cytological and/or histopathological 2-D microscopical images. Cytological smears are composed of isolated cells and/or 3-D clusters of cells. Nevertheless, the classical worldwide use of light microscopes for cancer diagnosis provides the cytopathologist with 2-D images. Clusters of overlapped cells may pose real diagnostic difficulties due to inappropriate distinction of the cellular features. Not infrequently, when a cytological smear contains such clusters of overlapped cells, the cytopathologist tries to gain some idea about the 3-D morphology of these clusters by rotating the micrometric knob. By doing so, the cytopathologist obtains optical serial images visualized at multiple lens foci. Usually, this manual procedure provides a limited amount of 3-D information about the cell/cluster morphology (the approach proposed in this work, although it deals with multiple foci as well, is capable of producing a significantly extended depth-of-focus range, which is more attractive for the information display, and it may be realized with an optically aided procedure requiring low computational complexity). Better methods for images with extended depth of focus are needed to obtain a clear distinction between the overlapped cells within a cluster. Such methods if used may significantly increase the diagnostic accuracy.

So far, in the field of cytopathology, a study conducted by Ramsamooj et al. compared 3-D imaging technology to the 2-D classical examination of cytological smears. Ramsamooj et al. tested the hypothesis that high-definition 3-D microscopy based on multiple oblique illumination (MOI), with its ability to penetrate into thick areas, would be useful

0091-3286/2006/$22.00 © 2006 SPIE

in evaluating problematic cervical Pap smears, particularly those diagnosed as atypical squamous cells of undetermined significance (ASCUS).[7] The authors found that 3-D microscopy based on MOI produced a superior diagnostic accuracy when compared with conventional light microscopy in evaluating cervical Pap smears ($P<0.001$). A different 3-D imaging technique applied in cytopathology was used by Boon et al.[8] The authors used confocal and fluorescent microscopy applied on PaP smears to perform 3-D reconstructions of the nuclei and mitotic figures. Using these methods and sophisticated computer software, the authors obtained a better resolution and gained valuable diagnostic information. A special diagnostic challenge would be the recognition of the primary origin of a metastatic cancer cell. Accurate 3-D techniques may contribute to the recognition of the primary origin of the metastatic cells.

In contrast to cytopathology (the study of cells), where whole free-floating cells are examined, histopathology is the study of tissues. In histopathology, thin (4 μm thick) tissue sections are performed and stained before the examination. The diagnosis in this case relies on the combined evaluation of the 2-D architectural patterns of the tissue elements along with the cytological features. As in cytology, not infrequently the pathologist needs volumetric information for an accurate diagnosis. Unlike in the cytological smears, observing the tissue section by various foci will not provide any additional information, since the section is very thin and per definition is considered to be a true 2-D specimen. Therefore, to gain some volumetric information (as well as to detect additional features), the pathologist performs multiple successive serial sections through the tissue sample and examines them one by one, imagining the continuation between the slices. The pathologist performs in this case a mental 3-D reconstruction of the examined tissue specimen. Thus, in this case a large amount of data exists. These data need to be processed and evaluated. For this case of histopathological diagnosis, optically aided compression using wavelet transform may be of a great benefit.

In this work, we suggest extracting high resolution in all dimensions (transversal and axial) by generating increased depth of focus without reducing the transversal resolution, and allowing efficient information handling by realizing optically aided data compression without the requirement of any computational complexity. The optically aided approach for obtaining increased depth of focus, together with higher spatial resolution as well as the data compression, is obtained using wavelet transformation. Note that the realized extended depth of focus could be used for display of 3-D information. Note also that extended depth of focus actually means super-resolving imaging, since getting out of focus means suppressing the high band spatial frequencies within the image. The wavelet transformation is performed in an optical manner just by proper subtracting of adjacent defocused images, while the out-of-focus images are obtained with a fast 3-D stepper in the axial z direction on which the diagnosed sample is placed.

There are various approaches for optical realization of wavelet transforms. Most work on optical wavelet transform has been done with coherent light. Techniques involving correlators based on filters and coherent light illumination were tested.[9–11] Another use of optical wavelet transform was done by Freysz et al.[12] using an optical correlator for identifying fractal aggregates relying on the scale property of the wavelet transform. Roberge et al.[13] used a time-varying holographic filter in the Fourier plane (again with coherent illumination). An acousto-optic modulation technique was used by Lu et al.[14] In Refs. 15 and 16, the wavelet transform was realized by wavelength multiplexing. Using Dammann grating and a computer-generated matched filter, another technique for wavelet decomposition was performed.[17]

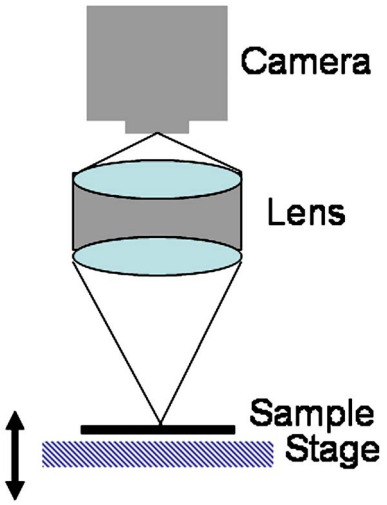

Fig. 1 The experimental optical system.

In Sec. 2, we briefly describe the definition and method of computing the optical transfer function. In Sec. 3, we focus on the theory of optically aided data manipulation. Section 4 deals with the experimental results related to extended depth of focus in cytological reconstruction, and in Sec. 5 we present an experimental investigation of optically aided wavelet compression of histological samples. The manuscript is concluded in Sec. 6.

2 Optical Transfer Function

The size of the aperture of the imaging lens determines the spatial resolution as well as the depth of focus of that imaging system. Spatial resolution of an imaging system is inversely related to the depth of focus. Increasing the aperture increases the spatial resolution but decreases the depth of focus and vice versa. Various approaches for extending the depth of focus are coming to break this tradeoff.[18–21] The optical transfer function (OTF) of the imaging system depends on the ratio between the focal lengths of the lens and the distances between the detector and the lens and the object and the lens (this is called the imaging condition). Infringing the imaging condition leads to narrowing of the OTF. The OTF is actually a filtering function that multiplies the spatial spectrum of the imaged object. The imaging condition can be easily infringed using a controlled shift of a 3-D stepper on which the sample is placed, in the axial z direction. Briefly, our approach includes applying proper subtraction and summation operations over the taken images, while controlled infringing of the imaging condition is realized, allowing the generation of spatial-spectral filtering following wavelet transform

decomposition.[9–17] This decomposition can be used for obtaining highly resolved increased depth of focus cytological images and an optically aided compression for histological samples.

The derivation of the OTF of a defocused circular pupil with an arbitrary diameter is based on an earlier calculation for a circular aperture with a normalized diameter performed by Hopkins in 1955.[22] The OTF of a diffraction-limited incoherent system is defined as:

$$H(f_x,f_y;Z_i)=\frac{\iint P\left(x+\frac{\lambda Z_i f_x}{2},y+\frac{\lambda Z_i f_y}{2}\right)P^*\left(x-\frac{\lambda Z_i f_x}{2},y-\frac{\lambda Z_i f_y}{2}\right)dxdy}{\iint |P(x,y)|^2 dxdy}, \tag{1}$$

where f_x and f_y are the coordinates of the 2-D OTF function, and Z_i is the distance between the lens and the sensing device. While in focus, $P(x,y)$ is the binary pupil function, which is "one" within the pupil, and zero outside. In this case, the OTF is simply:

$$H(f_x,f_y)=\frac{\text{Area of overlap}}{\text{Total area}}=\frac{\iint_{A(f_x,f_y)} dxdy}{\iint_{A(0,0)} dxdy}, \tag{2}$$

where $A(f_x,f_y)$ is the area of overlapping between two shifted pupils. When aberrations are introduced, the generalized pupil function can be described as:

$$P(x,y)=|P(x,y)|\exp[\mathrm{jkW}(x,y)], \tag{3}$$

where $W(x,y)$ is the wave aberration and $k=2\pi/\lambda$, where λ is the optical wavlength. Note that $P(x,y)$ is the generalized pupil function, while $|P(x,y)|$ is the binary function, which is "one" within the pupil and zero outside as before, and $W(x,y)$ is a phase aberation term added due to distortion, such as defocusing. If the aberrations are caused only by defocusing, $W(x,y)$ has the form of:

$$W(x,y)=W_m\frac{(x^2+y^2)}{R^2}, \tag{4}$$

where R is the radius of the aperture and the coefficient W_m determines the severity of the error:

$$W_m=\frac{R^2}{2Z_iZ_a}\Delta Z, \tag{5}$$

where ΔZ stands for Z_i-Z_a, where Z_a is the actual distance between the lens and the sensing device and Z_i is the distance between the lens and the sensing device when the object is in focus. For computing the OTF, we need to substitute the generalized pupil function of Eq. (3) into Eq. (1). Note that Eq. (4) was obtained using the paraxial approximation.

2.1 *Optical Transfer Function Derivation for Circular Pupil*

Following Ref. 22 and after proper mathematical derivation, we can write the defocused OTF as:

$$\begin{aligned}H(\rho)=&\frac{4}{\pi S\cdot R}\cos\left(S\frac{|\rho|}{2}\right)\left\{\beta J_1(S\cdot R)+\frac{1}{2}\sin(2\beta)[J_1(S\cdot R)\right.\\&-J_3(S\cdot R)]-\frac{1}{4}\sin(4\beta)[J_3(S\cdot R)-J_5(S\cdot R)]\\&\left.+\ \ldots\right\}\\&-\frac{4}{\pi S\cdot R}\sin\left(a\frac{|\rho|}{2}\right)\left\{\sin(\beta)[J_0(S\cdot R)-J_2(S\cdot R)]\right.\\&-\frac{1}{3}\sin(3\beta)[J_2(S\cdot R)-J_4(S\cdot R)]+\frac{1}{5}\sin(5\beta)\\&\left.\times[J_4(S\cdot R)-J_6(S\cdot R)]-\ \ldots\right\},\end{aligned} \tag{6}$$

where J_n are Bessel functions of the first type,

$$S=2k\frac{W_m}{R^2}\lambda Z_i f_x,\quad \beta=\arccos\left(\frac{|\rho|}{2R}\right),$$

and $\rho^2=f_x^2+f_y^2$. As previously menitoned, λ is the optical wavelength and $k=2\pi/\lambda$. R is the radius of the aperture of the imaging lens.

2.2 *One-Dimensional Pupil Optical Transfer Function Derivation*

In the 1-D case (cylindrical lens), Eq. (2) becomes:

$$H(f_x)=\left(1-\frac{|f_x|}{2f_{\mathrm{co}}}\right)\mathrm{sinc}\left[\frac{8W_m\pi}{\lambda}\left(\frac{f_x}{2f_{\mathrm{co}}}\right)\left(1-\frac{f_x}{2f_{\mathrm{co}}}\right)\right], \tag{7}$$

where the coherent cut-off spatial frequency is $f_{\mathrm{col}}=R/\lambda Z_a$, where the diameter of the lens is $2R$ and Z_a is the actual distance between the lens and the sensing device. The 1-D OTF while in focus is therefore:

$$H(f_x) = \left(1 - \frac{|f_x|}{2f_{co}}\right). \tag{8}$$

3 Optically Aided Data Manipulation

Our approach includes applying proper subtraction and summation operations over the taken images, while controlled infringing of the imaging condition is realized. This allows generating spatial-spectral filtering following the wavelet transform decomposition. This decomposition can be used for obtaining highly resolved increased depth-of-focus cytological images and an optically aided compression for histological samples.

We start by explaining the optically aided wavelet transforming technique using optical defocusing. Then, we describe the algorithm of how to use this approach for extended depth of focus in cytological images. Then, we use it for compression of histological samples. As previously mentioned, all of the suggested ingredients are to be used for approaching the defined objectives and goals.

3.1 *Wavelet Transform*

The continuous-time wavelet transform (CWT) of $f(t)$ with respect to a mother wavelet $\psi(t)$ is defined as:

$$W(a,b) \equiv \int_{-\infty}^{\infty} f(t)\psi_{a,b}^{*}(t)dt, \tag{9}$$

where

$$\psi_{a,b}(t) \equiv \frac{1}{\sqrt{|a|}}\psi\left(\frac{t-b}{a}\right), \tag{10}$$

where a is the scale of the function and b is the shift along the axis. Just to set all of the notations right, the function $\psi(t)$ is denoted as the mother wavelet, the wavelet transform $W(a,b)$ is also denoted as the wavelet coefficents, and Ψ_{ab} is the wavelet basis. In the following equations, the function f was time dependent, but obviously in our case the functions are space dependent.

The inverse wavelet transform can be computed as well if the mother wavelet function has a zero DC component. When we receive discrete values of scaling factors, the inverse wavelet is called the hybrid inverse wavelet transform and can be written as:

$$f(t) = \frac{1}{C}\sum_{a=-\infty}^{\infty}\frac{1}{|a|^2}\int_{b=-\infty}^{\infty} W(a,b)\psi_{a,b}(t)db, \tag{11}$$

where C is a constant and the scaling a usually goes as powers of 2.

Thus, to summarize this subsection, we can see that scaling and shifting the mother wavelet functions provides the wavelet basis Ψ_{ab}. Its multiplication and summation with the function that is to be transformed provides the wavelet coefficients $W(a,b)$. Multiplying and summing those coefficients with the wavelet basis provides the reconstruction of the original function [see Eq. (11)].

3.2 *Optically Aided Compression and Extended Depth of Focus: Theory*

Now we show how, by low complexity operations such as substraction and summation, we realize optical wavelet transformation for compresing information or use it for generation of extended depth-of-focus imaging. The optical wavelet transform is obtained by capturing microscopic images at different focusing ranges. Another option for the same outcome is capturing several images with an objective lens having the same magnification but varying in numerical aperture. Figure 1 presents an example for such a system. It consists of a camera, a lens, and a sample placed on top of a stage (stepper). The out-of-focus images are obtained with a fast 3-D stepper in the axial z direction, on which the diagnosed sample is placed.

The basic concept is based on the fact that subtracting the normalized OTF that affected each two adjacent defocused images yields wavelet basis functions $\psi_{a,b}(t)$ that resemble the Mexican hat. Assuming that one captures N $(0<i<N)$ defocused images, the larger the index i the more defocused the image is. For index $i=0$, the image is in focus. Subtraction of different adjacent planes (with different index i) varies the scaling of the mother wavelet functions:

$$\psi_{a_i,b}(t) = IFFT[\mathrm{OTF}(i) - \mathrm{OTF}(i+1)], \tag{12}$$

where the scaling factor a depends on the index i. Thus, subtraction of the images obtained from each two consecutive out-of-focus planes results in the proper wavelet coefficent $W(a_i,b)$:

$$W(a_i,b) = \mathrm{Im}_{\mathrm{detector}}(i) - \mathrm{Im}_{\mathrm{detector}}(i+1). \tag{13}$$

Note that an image obtained on a sensing device was spatial-spectrally filtered by the OTF of the respective defocusing: $\mathrm{Im}_{\mathrm{detector}}(i) = \mathrm{Im}_{\mathrm{object}} * IFFT[\mathrm{OTF}(i)]$. where $*$ denotes convolution operation, and thus one obtains:

$$\begin{aligned} W(a_i,b) &= \mathrm{Im}_{\mathrm{object}} * \{IFFT[\mathrm{OTF}(i)] - IFFT[\mathrm{OTF}(i+1)]\} \\ &= \mathrm{Im}_{\mathrm{object}} * \mathrm{FFT}[\psi_{a_i,b}(t)]. \end{aligned} \tag{14}$$

Having the basis functions and their scales allows us to reconstruct the image by applying the hybrid inverse wavelet transform [Eq. (11)]. The main point is that the accesability to the wavelet transform plane, which is obtained by almost all-optical means (except the substraction operations), can be used for the realization of image compression to obtain a fast rate of information transmission to the pathologic decision consulting center or to store the compressed information. The wavelet transform information may be inversed by digital computing of the inverse transform in the consultation center (the place to where all the information from the varios laboratories arrives). But, as mentioned before, the wavelet transform can be used not only for the compression of information but also for the realization of extended depth of focus. The summation of the various wavelet basis functions can lead to spatial-spectral transmission, which is wider than any individual wavelet basis function or any individual OTF, and is more or less constant for the different defocusing positions of the object.

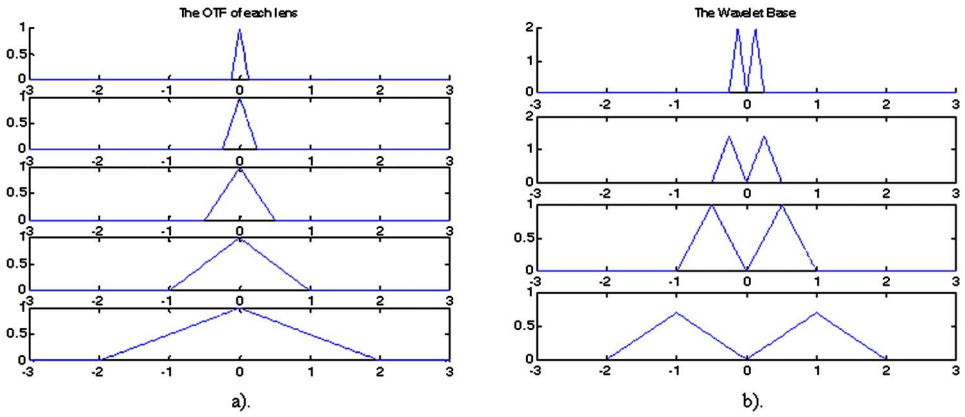

Fig. 2 (a). The OTF of lenses with varying diameters. (b). The wavelet basis that can be constructed by the subtraction of the OTF of (a).

Note that the same results can be obtained if instead of a set of defocused images one captures a set of images while the numerical aperture of the imaging lens is varied from image to image. Since in the hybrid wavelet transform the scale factor a goes as powers of 2, the numerical aperture should be varied by a factor of 2 each time.

To demonstrate the expressions appearing in Eqs. (12)–(14), in Fig. 2(a) we present what the OTF of a set of lenses with numerical apertures varied by a factor of 2 each time looks like. In Fig. 2(b) we present the corresponding images obtained when two adjacent OTFs are subtracted each time. As seen from Fig. 2(b), the results resemble very much the Mexican-hat wavelet basis and thus can be used for wavelet compressing the images. Similar results can be obtained when a set of defocused images are captured. There also a Mexican-hat-like basis is obtained. By proper choice of summation of the obtained wavelet coefficients, one may obtain extended depth of focus. Note that although the object is a 3-D object and the defocusing function is a 3-D function as well, and since the hybrid wavelet trans-

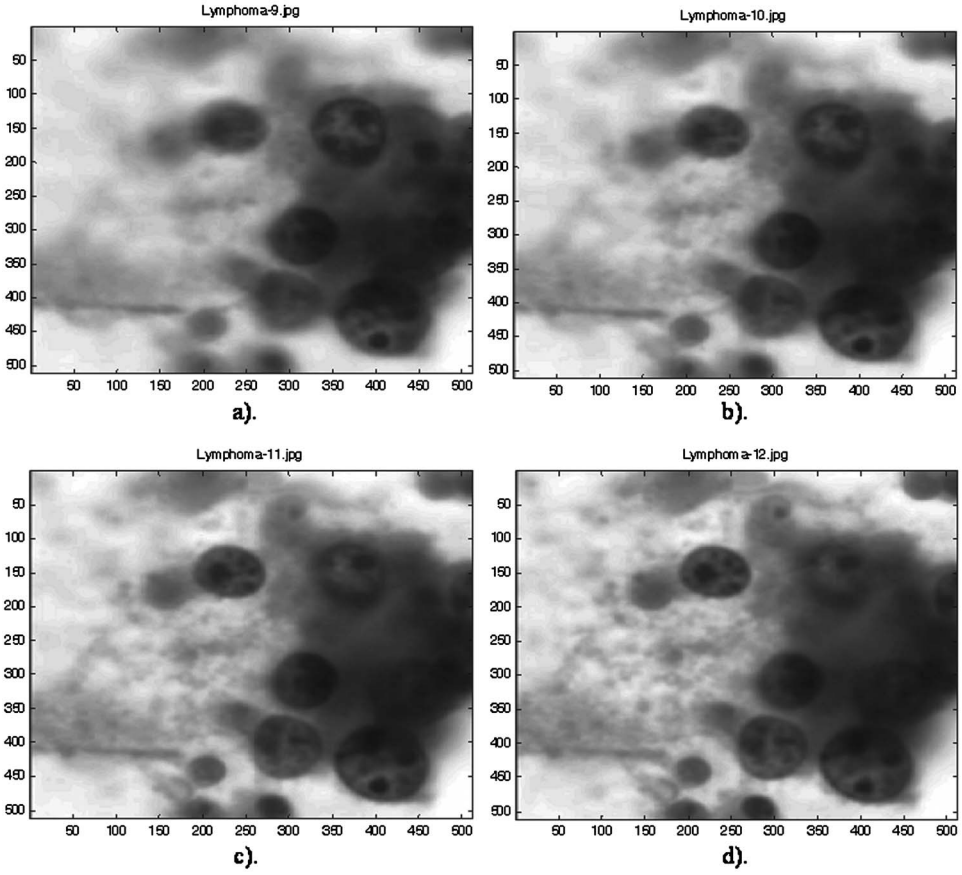

Fig. 3 Original cytological 2-D images.

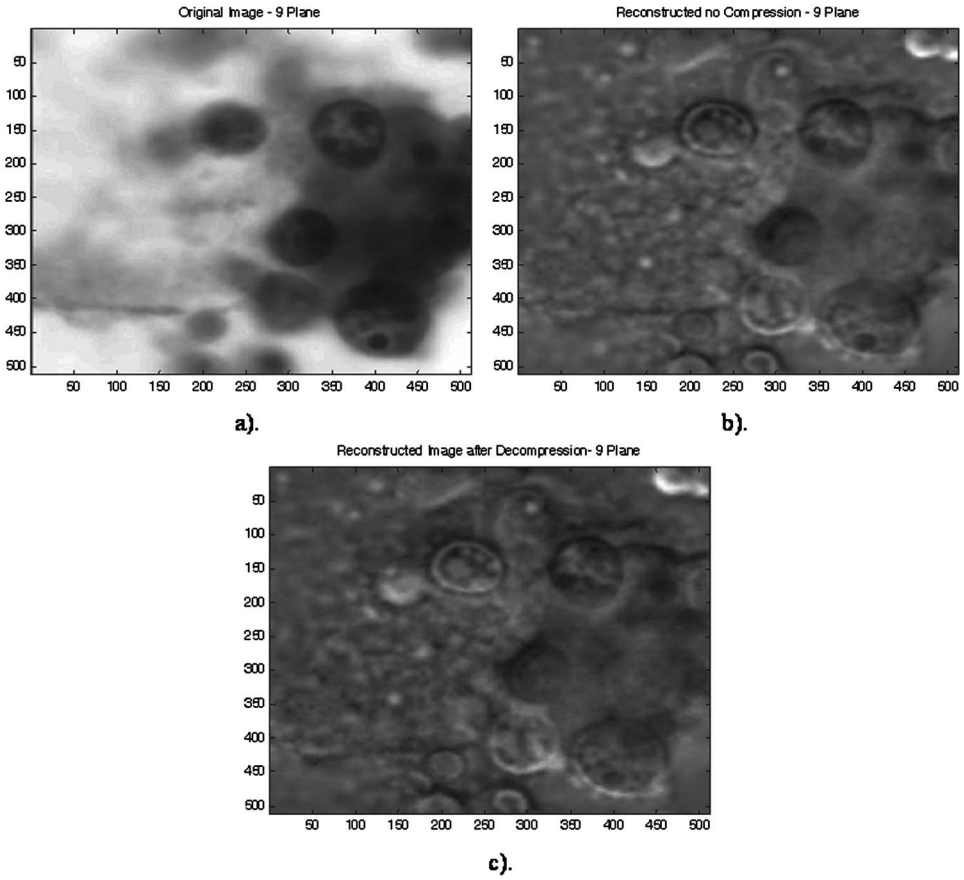

Fig. 4 (a) The original image of plane 9 in focus. (b) The increased depth-of-focus generation. (c) The reconstruction after a compression factor of 2.9948.

form can provide compression and reconstruction as well as the continuous wavelet transform, we make the 3-D blurring function of defocusing discrete by choosing discrete images for the subtraction while the axial position of those images produce scales of the OTF each time by a factor of 2. Note also that in all of our analysis, we have assumed the scalar theory of waves rather than the vectorial representation. This assumption is correct, since in our experiments the spatial content of the object does not include details close to the optical wavelength λ.

4 Extended Depth of Focus in Cytological Reconstruction

As previously mentioned, the cytological samples have 3-D structure that causes the defocusing of certain items in the image when the focus position of the microscope is varied. In this section we experimentally present the usage of the previously described defocusing technique for obtaining cytological images with extended depth of focus (obviously, as before, by performing low complexity operations such as summations and subtraction). Note that increased depth of focus means that one may improve the spatial resolution of the microscope and have the same depth of focus as before the improvement by using lenses with larger NA, so the depth of focus strongly relates to super-resolution (the depth of focus is proportional to λ/NA^2 and the maximal resolvable spatial frequency is proportional to NA/λ.

The figures present some preliminary experimental results using cytological smears containing lymphoma cells (i.e., malignant cells originating in the lymphatic system), stained by the Papanicolau method. The pictures correspond to a one-micron shifting in the focus plane. Adjacent OTFs for the 2-D images at each distance were subtracted to generate the wavelet basis functions for the increased depth of focus and for compression. Some of the original images are presented in Fig. 3.

The generation of extended depth of focus performed in comparison to the image in Fig. 4(a) is depicted in Fig. 4(b), and it is obtained by multiplying the wavelet coefficients with the basis functions and summing them together. By enhancing the proper coefficients, 2-D images of different focal planes may be obtained. If in the process of wavelet decomposing a decimation is introduced, a compression is obtained for the depth-of-focus enhanced images, as presented in Fig. 4(c).

Figures 5–7 are similar to Fig. 4; however, each one presents the enhanced depth-of-focus generation and compression around different focus planes. Figure 4 was for plane number 9, and Figs. 5–7 were for planes 6, 3, and 0, respectively. Note that the number for the in-focus plane

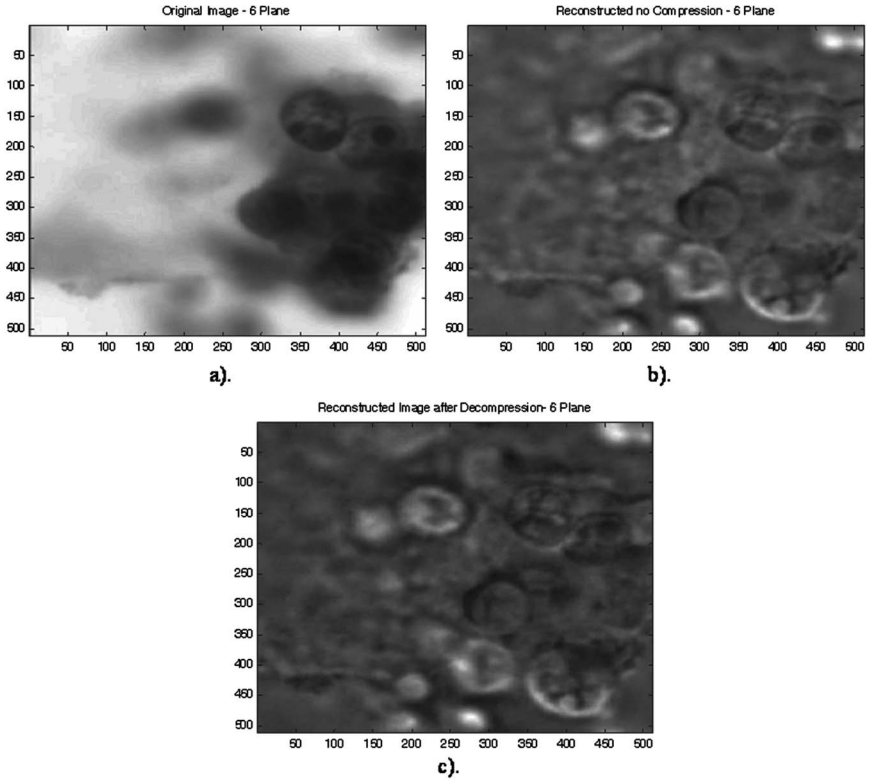

Fig. 5 (a) The original image of plane 6 in focus. (b) The generation of increased depth of focus. (c) The reconstruction after a compression factor of 3.0009.

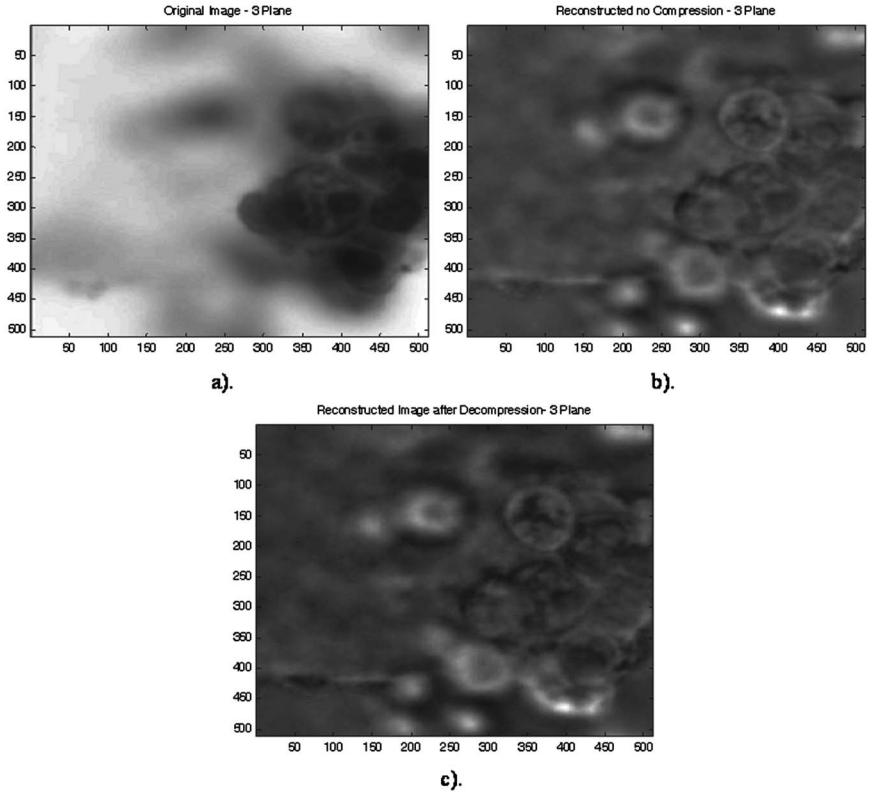

Fig. 6 (a). The original image of plane 3 in focus. (b) The generation of increased depth of focus. (c) The reconstruction after a compression factor of 3.0005.

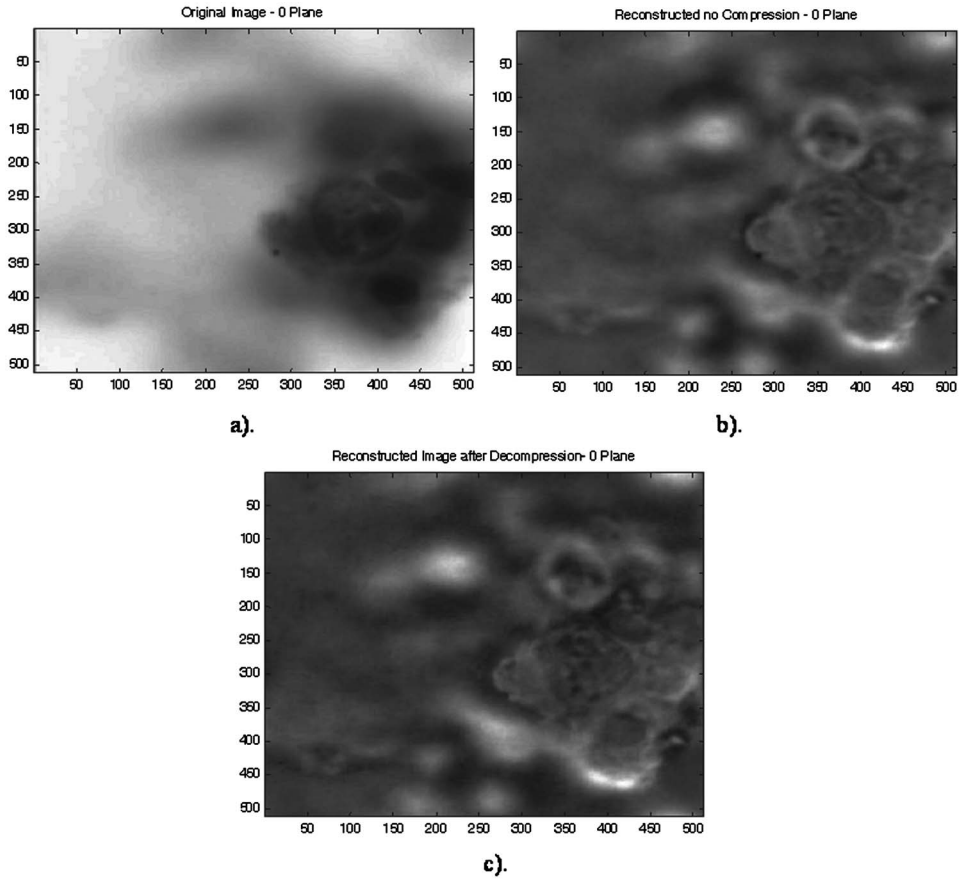

Fig. 7 (a) The original image of plane 0 in focus. (b) The generation of increased depth of focus. (c) The reconstruction after a compression factor of 3.0107.

corresponds to a 1-μm shift of the plane. In all the figures, we present the extended depth-of-focus image obtained also after applying the optically aided wavelet compression, and afterward image reconstruction (recomposing the image out of the thresholded and decimated wavelet coefficients). In all cases, a compression factor of approximately three times the compression was obtained.

5 Optically Aided Wavelet Compression of Histological Samples

In this section, we use the optical wavelet transform due to defocus to compress 2-D histological images. Once again by performing subtraction between the defocused images, the wavelet coefficients may be extracted and used for optically aided compression [see Eq. (14)]. In Fig. 8, we present the original image obtained from a 4-μm-thick prostatic tissue section, stained by hematoxylin and eosin.

The OTF of the imaging system changes as the image becomes out of focus. When choosing the appropriate distances for the object or the proper amount of defocusing, one can have OTFs with cut-off frequencies scaled by a factor of 2 (see Fig. 2). In this case, by subtracting each two consecutive images and scaling them, wavelet coefficients are received as depicted in Figs. 9(a)–9(f) (the figure presents the first six coefficients). The theoretical justification for the fact that subtraction of the adjacent defocused images provides a Mexican-hat resembling wavelet basis functions may be seen in Fig. 2 and discussed in Sec. 3.

The reconstructed image from the original wavelet coefficients is presented in Fig. 10. This is the image obtained without compression. Obviously, it is similar to the original

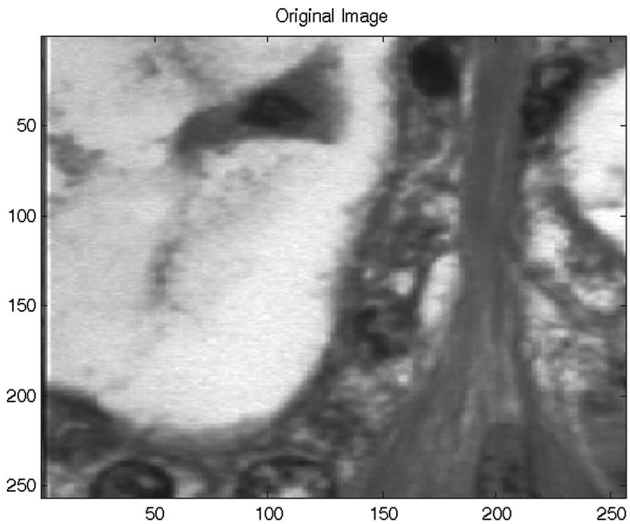

Fig. 8 Histological experimental image sample.

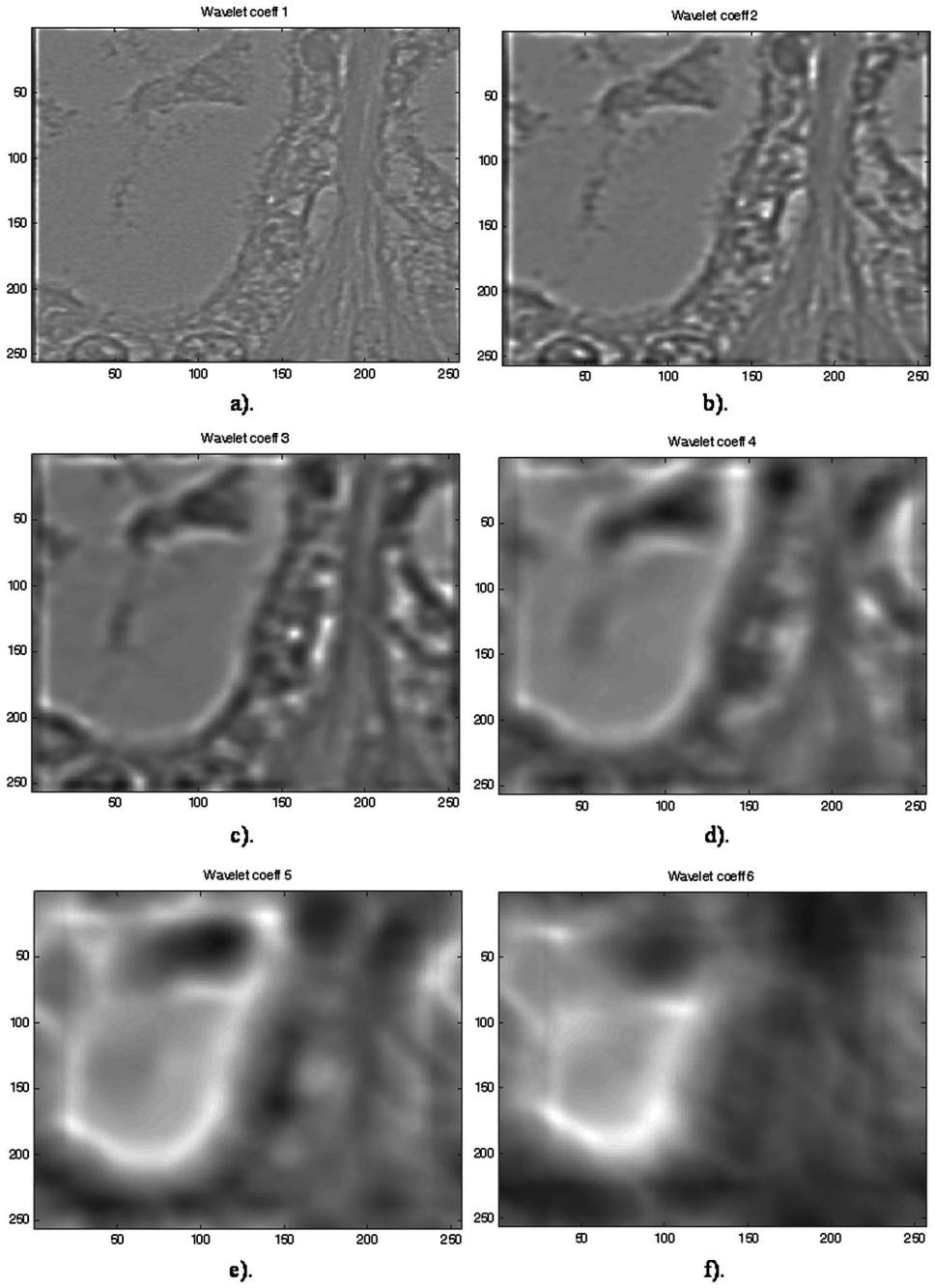

Fig. 9 (a) through (f) six wavelet coefficients obtained by optically taking the image out of focus and subtracting adjacent images.

one. The reconstruction is obtained by digital performing of the inverse wavelet transform [following Eq. (11)].

For compression, the optically obtained wavelet coefficients of Figs. 9(a)–9(f) were decimated and then compressed using run length encoding (RLE) with a compression ratio of 2.972. This digital procedure was done following the format of JPEG-2000. In this compression engine, a wavelet transform is applied on the image. The output of the transform is a set of coefficients that hold the information about the image in a representation that is more appropriate for compression. The coefficients are then quantized and compressed using a compression algorithm (e.g., RLE).

The RLE is based on the idea that consequential appearance of the same character may be compressed by replacing its multiple appearances by the character and the number indicating its number of appearance. For instance, when the wavelet transform is used and the quantization is applied, many zeros appear in the image. Instead of having all of them, one may save in his file only the digit zero and next

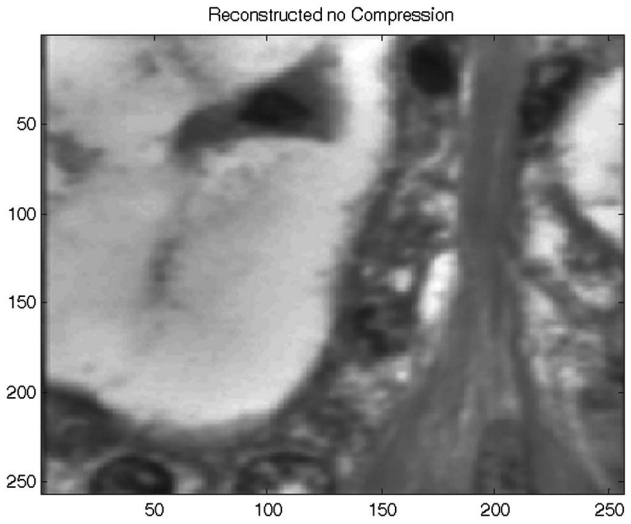

Fig. 10 The reconstructed image.

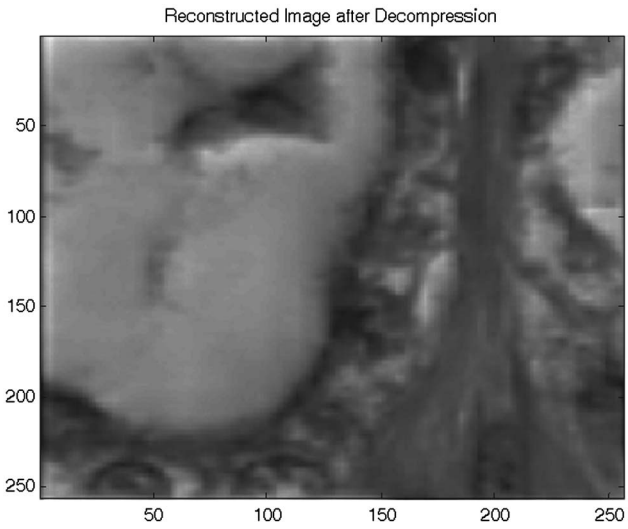

Fig. 11 Reconstructed image after decompression.

to it a digit indicating the number of the zero's appearance. Obviously, this rule can be applied to any number, not only zero. As an example, one may relate to the following sequence: 12 13 13 13 13 14 14 14 14 0 0 0 0 0 0 9 9 9 0. This sequence will be coded with: 12 ! 4 13 ! 4 14 ! 5 0 9 9 9 0. Where ! is the control character indicating that replacement occurred. Note that if the number of the sequential numbers is two or less, the previously explained rule does not apply and the numbers appear unchanged.

Reconstruction of the image out of the compressed wavelet coefficients requires decompression of the coefficients using an RLE decoder. Applying the inverse wavelet transform to the coefficients will result with the reconstructed image. Note that the compression algorithms are divided into two groups: lossless and lossy image compression. The lossless compressions do not lose any information from the original data (RLE is an example of such a compression). The transform used before the compression (i.e., discrete wavelet transform) does not damage the information as well. When introducing quantization, data are lost and the compression is then called lossy.

Note also that the main outcome of this experiment was not the compression itself but rather the fact that it was obtained by optical means with negligible digital processing complexity. The compression factor of 2.972 was obtained, while the allowed mean square error normalized by the number of pixels was not more than one gray level:

$$\varepsilon = \frac{1}{M}\left\{\sum_{m=1}^{M}[r(m)-f(m)]^2\right\} < 1,$$

where r is the reconstructed image after the compression and decompression and f is the original image. m is the number of pixels and M is the total number of pixels in the image. ε is the error that is less than one gray level. This obtained error also indicates how closely the subtraction of the OTFs of adjacent images provides the wavelet basis. Since the reconstruction error is so small, the subtraction indeed gives a basis that is very close to the desired wavelet basis.

The reconstructed image after decompression is seen in Fig. 11. One can see the similarity between the experimental results of Fig. 11 and the original image. This compression ratio of almost three was obtained by optically aided means with very low computation complexity, which involved only performing subtractions between out-of-focus captured images.

As previously mentioned, the out-of-focus images can be processed with a fast 3-D stepper in the axial z direction, and after performing optically aided compression, the images can be sent to a computation and analysis biomedical center, where they can be decompressed and processed at will.

6 Conclusions

We present an approach for obtaining an optically extended depth of focus and using it for 3-D display in microscopic pathological diagnostics. The extended depth of focus is used for cytological applications and is fulfilled using optically aided realization of wavelet transforms. Note also that extended depth of focus actually means axial superresolving imaging, since out of focus means suppressing the high band spatial frequencies within the image. A similar optical operation is also used for histological applications to obtain data compression with low computational complexity. We present the theory as well as experimental results demonstrating the capabilities of the suggested approach.

It is important to note that digital restoration microscopy is not a new topic, and the use of the wavelet transform does not claim to obtain a better performance than the one obtained using digital microscopy. The main claim presented is for an optical mean of realizing a wavelet transform with very low computational complexity and then its use for applications such as 3-D display (volume rendering by serial sectioning and not stereo projection), extended depth of focus, super resolution, and compression.

References

1. R. Ramsamooj, E. Doolin, G. Greenberg, E. Catalano, and C. W. Hawitt, "Real-time, high-definition, three-dimensional microscopy for evaluating problematic cervical Papanicolaou smears classified as atypical squamous cells of undetermined significance," *Cancer* **96**(3), 181–186 (2002).
2. P. Trk, Z. Laczik, and C. J. R. Sheppard, "Effect of half-stop lateral misalignment on imaging of dark-field and stereoscopic confocal microscopes," *Appl. Opt.* **35**, 6732 (1996).
3. S. Cha, P. C. Lin, L. Zhu, P. C. Sun, and Y. Fainman, "Nontranslational three-dimensional profilometry by chromatic confocal microscopy with dynamically configurable micromirror scanning," *Appl. Opt.* **39**, 2605–2613 (2000).
4. G. Pedrini and H. J. Tiziani, "Short-coherence digital microscopy by use of a lensless holographic imaging system," *Appl. Opt.* **41**, 4489–4496 (2002).
5. B. W. Schilling, T. C. Poon, G. Indebetouw, B. Storrie, K. Shinoda, Y. Suzuki, and M. H. Wu, "Three dimensional holographic fluorescence microscopy," *Opt. Lett.* **22**, 1506–1508 (1997).
6. W. A. Carrington, "Image restoration in 3-D microscopy with limited data," *Proc. SPIE* **1205**, 72–83 (1990).
7. R. Ramsamooj, E. Doolin, G. Greenberg, E. Catalano, and C. W. Hewitt, "Real-time, high-definition, three-dimensional microscopy for evaluating problematic cervical Papanicolaou smears classified as atypical squamous cells of undetermined significance," *Cancer* **25;96**(3), 181–186 (2002).
8. M. E. Boon, J. J. Schut, E. M. Benita, and L. P. Kok, "Confocal optical sectioning and three-dimensional reconstruction of carcinoma fragments in Pap smears using sophisticated image data processing," *Diagn. Cytopathol* **10**(3), 268–275 (1994).
9. Y. Sheng, D. Roberge, and H. Szu, "Optical wavelet transform," *Opt. Eng.* **31**(9), 1840–1845 (1992).
10. D. Mendlovic and N. Konforti, "Optical realization of the wavelet transform for two dimensional objects," *Appl. Opt.* **32**, 6542–6546 (1993).
11. H. Szu, Y. Sheng, and J. Chen, "The wavelet transform as a bank of matched filters," *Appl. Opt.* **31**, 3267–3277 (1992).
12. E. Freysz, B. Pouligny, F. Argoul, and A. Arneodo, "Optical wavelet transform of fractal aggregates," *Phys. Rev. Lett.* **V64**, 745–748 (1990).
13. D. Roberge, Y. Sheng, T. Lu, and H. J. Caulfield, "Optical N^4 implementation of a two-dimensional wavelet transform," *Opt. Eng.* **31**(9), 1859–1864 (1992).
14. X. J. Lu, A. Katz, E. G. Kanterakis, and N. P. Caviris, "Joint transform correlation using wavelet transforms," *Opt. Lett.* **17**, 1700–1703 (1992).
15. J. Garcia, Z. Zalevsky, and D. Mendlovic, "Two dimensional wavelet transform by wavelength multiplexing," *Appl. Opt.* **35**, 7019–7024 (1996).
16. Z. Zalevsky, "Experimental implementation of a continuous 2-D on axis optical wavelet transformer with white light illumination," *Opt. Eng.* **37**(4), 1372–1375 (1998).
17. D. Mendlovic, I. Ouzieli, I. Kiryuschev, and E. Marom, "A 2-D wavelet transform achieved by computer generated multireference matched filter and Dammann grating," *Appl. Opt.* **34**, 8213–8219 (1995).
18. E. R. Dowski Jr. and W. T. Cathey, "Extended depth of field through wave-front coding" *Appl. Opt.* **34**, 1859 (1995).
19. J. van der Gracht, E. R. Dowski Jr., M. G. Taylor, and D. M. Deaver, "Broadband behavior of an optical-digital focus-invariant system," *Opt. Lett.* **21**, 919–921 (1996).
20. N. George and W. Chi, "Extended depth of field using logarithmic asphere," *J. Opt. A, Pure Appl. Opt.* **5**, S157–S163 (2003).
21. E. Ben-Eliezer, Z. Zalevsky, E. Marom, and N. Konforti, "All-optical extended depth of field imaging system," *J. Opt. A, Pure Appl. Opt.* **5**, S164–S169 (2003).
22. H. H. Hopkins, "The frequency response of a defocused optical system," *Proc. R. Soc. London, Ser. A* **231**, 91–103 (1955).

Biographies and photographs of authors not available.